



# First observation of the $B^+ \rightarrow D_s^+ D_s^- K^+$ decay

LHCb collaboration

## Abstract

The  $B^+ \rightarrow D_s^+ D_s^- K^+$  decay is observed for the first time using proton-proton collision data collected by the LHCb detector at centre-of-mass energies of 7, 8 and 13 TeV, corresponding to an integrated luminosity of  $9 \text{ fb}^{-1}$ . Its branching fraction relative to that of the  $B^+ \rightarrow D^+ D^- K^+$  decay is measured to be

$$\frac{\mathcal{B}(B^+ \rightarrow D_s^+ D_s^- K^+)}{\mathcal{B}(B^+ \rightarrow D^+ D^- K^+)} = 0.525 \pm 0.033 \pm 0.027 \pm 0.034,$$

where the first uncertainty is statistical, the second systematic, and the third is due to the uncertainties on the branching fractions of the  $D_s^\pm \rightarrow K^\mp K^\pm \pi^\pm$  and  $D^\pm \rightarrow K^\mp \pi^\pm \pi^\pm$  decays. This measurement fills an experimental gap in the knowledge of the family of Cabibbo-favoured  $\bar{b} \rightarrow \bar{c} c \bar{s}$  transitions and opens the path for unique studies of spectroscopy in future.

Submitted to Phys. Rev. D



# 1 Introduction

The family of  $B \rightarrow D_{(s)}^{(*)} \bar{D}_{(s)}^{(*)} K^{(*)}$  decays proceeds at the quark level via the Cabibbo-favoured  $\bar{b} \rightarrow \bar{c} c \bar{s}$  transition.<sup>1</sup> Such decays provide an excellent laboratory for investigations of open- and hidden-charm meson spectroscopy, covering both conventional and exotic states. Additionally, measurements of the amplitude structures in the  $D_{(s)}^{(*)} \bar{D}_{(s)}^{(*)}$  system of these decays can offer important information to the theoretical calculations of the charm-loop contributions to  $b \rightarrow s \ell^+ \ell^-$  processes that are sensitive to physics beyond the Standard Model [1].

There have already been experimental studies of  $B \rightarrow D^{(*)} \bar{D}^{(*)} K^{(*)}$  decays by the ALEPH, BaBar, Belle and LHCb collaborations [2–13], not only making observations of some of these decay channels, but also leading to discoveries of new resonances. However, all such measurements to date focus only on  $B$  decays with a  $D^{(*)} \bar{D}^{(*)}$  pair in the final state. Decays involving the  $D_s^{(*)+} D_s^{(*)-}$  pair, *e.g.*  $B^+ \rightarrow D_s^+ D_s^- K^+$ , have never been explored. The  $D_s^+ D_s^-$  system is attractive as it provides a unique insight into the charmonium(-like) spectroscopy. Conventional charmonium mesons with natural spin ( $J$ ), parity ( $P$ ), and charge-parity ( $C$ ) quantum numbers ( $J^{PC} = 0^{++}, 1^{--}, 2^{++}, \dots$ ), *e.g.*  $\psi(4040)$  [14], are expected to predominantly decay into the  $D^{(*)} \bar{D}^{(*)}$  final state. In contrast, charmonium-like hadrons with the  $c\bar{c}s\bar{s}$  constituents could have a larger partial decay width to the  $D_s^+ D_s^-$  final state than that to  $D^{(*)} \bar{D}^{(*)}$ . A few candidates for  $c\bar{c}s\bar{s}$  states have been observed in the  $J/\psi\phi$  final state from  $B^+ \rightarrow J/\psi\phi K^+$  decays [15]. They might also decay into  $D_s^+ D_s^-$  and contribute to the  $B^+ \rightarrow D_s^+ D_s^- K^+$  decay.

This paper presents the first observation of the  $B^+ \rightarrow D_s^+ D_s^- K^+$  decay. The contributing tree-level Feynman diagrams of this decay are shown in Fig. 1. The branching fraction of the  $B^+ \rightarrow D_s^+ D_s^- K^+$  decay is measured relative to that of the normalisation channel  $B^+ \rightarrow D^+ D^- K^+$ . The two channels have a similar decay topology, so the corresponding systematic uncertainties on the branching-fraction ratio are expected to largely cancel. The measurement uses the proton-proton ( $pp$ ) collision data collected by the LHCb experiment in 2011, 2012 and 2015–2018 at centre-of-mass energies of 7, 8 and 13 TeV, respectively, corresponding to a total integrated luminosity of  $9 \text{ fb}^{-1}$ . The branching fraction of the  $B^+ \rightarrow D_s^+ D_s^- K^+$  decay is an essential input to obtain the partial width information of the

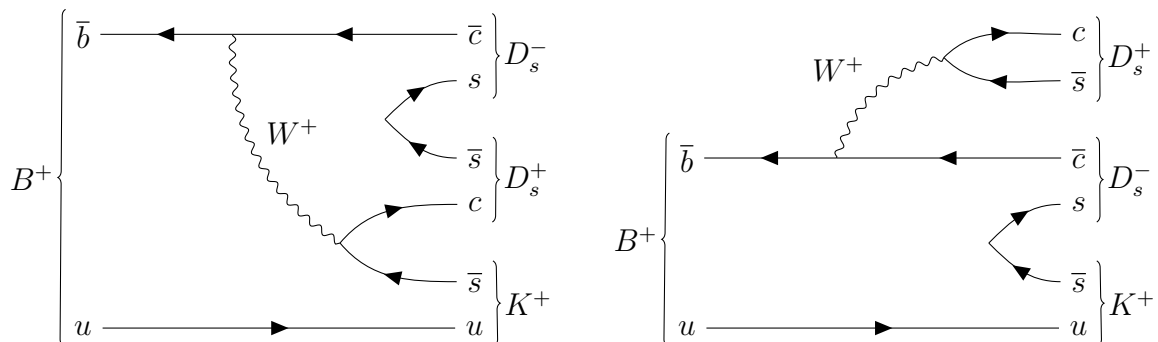


Figure 1: Feynman diagrams contributing to the  $B^+ \rightarrow D_s^+ D_s^- K^+$  decay.

<sup>1</sup>The inclusion of charge-conjugate modes is always implied and natural units with  $\hbar = c = 1$  are used throughout the paper.

near-threshold structure in the  $D_s^+ D_s^-$  system analysed in the accompanying paper [16].

## 2 Detector and simulation

The LHCb detector [17, 18] is a single-arm forward spectrometer covering the pseudo-rapidity range  $2 < \eta < 5$ , designed for the study of particles containing  $b$  or  $c$  quarks. The detector includes a high-precision tracking system consisting of a silicon-strip vertex detector surrounding the  $pp$  interaction region [19], a large-area silicon-strip detector located upstream of a dipole magnet with a bending power of about 4 Tm, and three stations of silicon-strip detectors and straw drift tubes [20, 21] placed downstream of the magnet. The tracking system provides a measurement of the momentum,  $p$ , of charged particles with a relative uncertainty that varies from 0.5% at low momentum to 1.0% at 200 GeV. The minimum distance of a track to a primary  $pp$  collision vertex (PV), the impact parameter, is measured with a resolution of  $(15 + 29/p_T) \mu\text{m}$ , where  $p_T$  is the component of the momentum transverse to the beam, in GeV. Different types of charged hadrons are distinguished using information from two ring-imaging Cherenkov detectors [22]. Photons, electrons and hadrons are identified by a calorimeter system consisting of scintillating-pad and preshower detectors, an electromagnetic and a hadronic calorimeter. Muons are identified by a system composed of alternating layers of iron and multiwire proportional chambers [23].

The online event selection is performed by a trigger [24], which consists of a hardware stage, based on information from the calorimeter and muon systems, followed by a software stage, which applies a full event reconstruction. At the hardware trigger stage, events are required to have a muon with high  $p_T$  or a hadron, photon or electron with high transverse energy in the calorimeters. The hadron can originate from either the studied decay or the rest of the event. The software trigger requires a two-, three- or four-track secondary vertex with a significant displacement from any PV. At least one charged particle must have a transverse momentum  $p_T > 1.6$  GeV and be inconsistent with originating from a PV. A multivariate algorithm [25, 26] is used for the identification of secondary vertices consistent with the decay of a  $b$  hadron.

Simulation is required to model the effects of the detector acceptance and the imposed selection requirements for the  $B^+ \rightarrow D_s^+ D_s^- K^+$  and  $B^+ \rightarrow D^+ D^- K^+$  decays. In the simulation,  $pp$  collisions are generated using PYTHIA [27] with a specific LHCb configuration [28]. Decays of unstable particles are described by EVTGEN [29], in which final-state radiation is generated using PHOTOS [30]. The interaction of the generated particles with the detector, and its response, are implemented using the GEANT4 toolkit [31] as described in Ref. [32]. The underlying  $pp$  interaction is reused multiple times, with an independently generated signal decay for each event [33]. The particle-identification (PID) response is not well described in the LHCb simulation, and is corrected to match that in data. The correction is determined from calibration samples using a reweighing approach, the so-called PID transformation [34, 35].

## 3 Event selection

The  $B^+ \rightarrow D_s^+ D_s^- K^+$  and  $B^+ \rightarrow D^+ D^- K^+$  decays are reconstructed using the  $D_s^+ \rightarrow K^+ K^- \pi^+$  and  $D^+ \rightarrow K^- \pi^+ \pi^+$  decay channels, respectively. The selection starts

by choosing well-reconstructed tracks that are inconsistent with originating from any PV. The selected tracks should have PID information consistent with the corresponding final-state kaons and pions. Additionally, the opening angle between any two final-state charged tracks must be larger than 0.5 mrad to reduce potential reuse of track segments. The  $D^+$  and  $D_s^+$  candidates, obtained by combining  $K$  and  $\pi$  candidates, are required to have good-quality vertices and their reconstructed masses should lie within  $\pm 25$  MeV of the known masses [14]. The  $B^+$  candidates are then formed by combining  $D_{(s)}^+$ ,  $D_{(s)}^-$  and  $K^+$  candidates. The  $B^+$  decay vertex must be well reconstructed and significantly displaced from all PVs. The  $B^+$  candidate is required to have a flight direction pointing back to the PV where it is produced, referred to hereafter as the associated PV. To reduce the contamination from the non-double-charm (NDC)  $B^+$  decay candidates that have the same set of the final-state tracks as that of the  $B^+ \rightarrow D_{(s)}^+ D_{(s)}^- K^+$  decay but do not involve two real  $D_{(s)}^\pm$  mesons, requirements on the distances between the  $B^+$  and  $D_{(s)}^\pm$  vertices are imposed, taking advantage of the nonzero flight distance of the  $D_{(s)}^\pm$  meson. A kinematic fit [36] is employed to improve the  $B^+$  mass resolution by constraining the  $D_{(s)}^\pm$  mass to its known value [14] and requiring the  $B^+$  candidate to originate from the associated PV. A second kinematic fit with an additional  $B^+$  mass constraint is utilised when investigating the distributions of the Dalitz-plot variables in  $B^+ \rightarrow D_s^+ D_s^- K^+$  and  $B^+ \rightarrow D^+ D^- K^+$  decays.

Gradient Boosted Decision Tree (BDTG) [37–39] classifiers are employed to reduce further background from random combinations of tracks, referred to hereafter as combinatorial background. The classifier is trained separately for the  $B^+ \rightarrow D_s^+ D_s^- K^+$  and  $B^+ \rightarrow D^+ D^- K^+$  channels using the corresponding simulated sample as the signal proxy and candidates in data with a reconstructed  $B^+$  mass of 5360 – 6000 MeV as the background proxy. The discriminating variables used in the classifier include PID information of the final-state tracks, kinematic properties and the decay topology of the  $B^+$  and  $D_{(s)}^\pm$  candidates. The selection criterion for the response of each classifier is optimised by maximising the figure of merit,  $N_S/\sqrt{N_S + N_B}$ , separately for each channel. Here,  $N_S$  ( $N_B$ ) is the expected signal (background) yield within  $\pm 20$  MeV of the known  $B^+$  mass [14], estimated as the product of the signal (background) yield without any BDTG requirement and the signal efficiency (1 – background-rejection factor) for a given criterion. The signal and background yields without the BDTG requirements in each channel are evaluated using a simple fit to the reconstructed  $B^+$  mass distribution with the signal and background probability density functions (PDF) modelled by a Gaussian function and an exponential function, respectively. The signal efficiency and background-rejection factor are directly obtained from the samples used to test the classifiers.

Multiple candidates, found in a few percent of  $pp$  collision events, are mostly due to the duplicated use of tracks from the same event. In each event, the candidate having the smallest  $\chi^2$  of the kinematic fit without the  $B^+$  mass constraint is retained.

The reconstructed  $D_s^+ D_s^- K^+$  and  $D^+ D^- K^+$  invariant-mass distributions after all the selection requirements are shown in Fig. 2. The mass windows, (5280 – 80, 5280 + 80) MeV and (5280 – 60, 5280 + 80) MeV, for the signal and normalisation channels, respectively, are chosen to exclude the contributions of partially reconstructed background with a missing photon from  $D_s^{*\pm} \rightarrow D_s^\pm \gamma$  or  $D^{*\pm} \rightarrow D^\pm \gamma$  decay. Here, the tighter lower-side threshold for the  $B^+ \rightarrow D^+ D^- K^+$  channel than that for the  $B^+ \rightarrow D_s^+ D_s^- K^+$  channel is found necessary to exclude all visible tails of the partially reconstructed background [11,12].

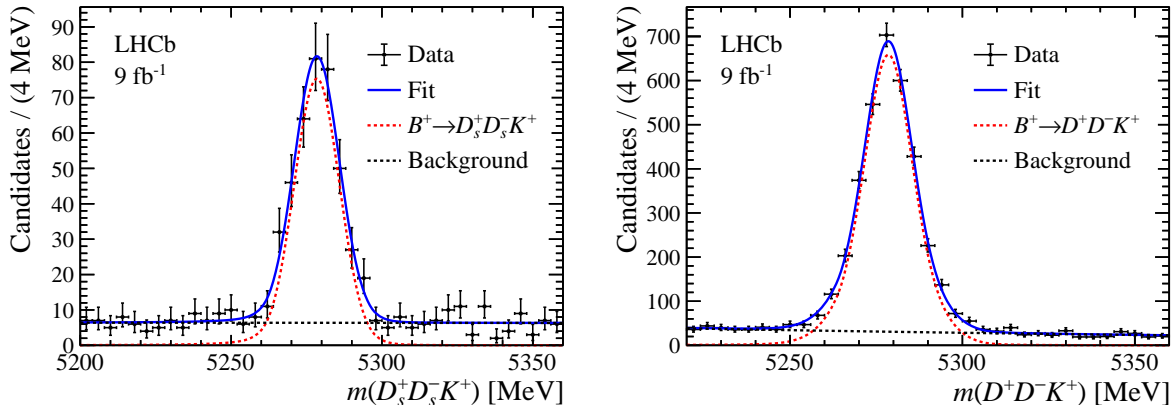


Figure 2: Invariant-mass distributions of reconstructed (left)  $D_s^+ D_s^- K^+$  and (right)  $D^+ D^- K^+$  candidates. The fit results are overlaid.

These mass windows are also sufficient to exclude partially reconstructed background with a missing  $\pi^0$  meson from  $D_s^{*+} \rightarrow D_s^+ \pi^0$  or  $D^{*+} \rightarrow D^+ \pi^0$  decay, as the reconstructed  $D_s^+ D_s^- K^+$  or  $D^+ D^- K^+$  mass is shifted at least 135 MeV below the  $B^+$  mass peak [14]. For both the  $B^+ \rightarrow D_s^+ D_s^- K^+$  signal and  $B^+ \rightarrow D^+ D^- K^+$  normalisation channels, any potential background resulting from the misidentification of a single  $K$  or  $\pi$  would originate from Cabbibo-suppressed decays and thus is negligible.

## 4 Signal extraction

Unbinned extended maximum-likelihood fits to the mass distributions of the  $B^+$  candidates are performed to determine the signal yields in the  $B^+ \rightarrow D_s^+ D_s^- K^+$  and  $B^+ \rightarrow D^+ D^- K^+$  channels. The signal PDF is a sum of two Crystal Ball (CB) functions [40] with a common peak position and opposite-side tails. The tail parameters are fixed to the values obtained from the simulated  $B^+ \rightarrow D^+ D^- K^+$  or  $B^+ \rightarrow D_s^+ D_s^- K^+$  sample. The combinatorial background is modelled using an exponential function.

The fit results are shown in Fig. 2. A signal yield of  $N_{\text{sig}} = 360 \pm 22$ , where the uncertainty is statistical only, is obtained for the  $B^+ \rightarrow D_s^+ D_s^- K^+$  decay, with a purity in a  $\pm 20$  MeV window around the peak of approximately 84%. The statistical significance is much larger than 10 standard deviations ( $\sigma$ ). Since the systematic uncertainty discussed in Sec. 6 is expected not to reduce the significance much, this result leads to the first observation of the  $B^+ \rightarrow D_s^+ D_s^- K^+$  decay. Here, the statistical significance is evaluated under the assumption that the log-likelihood difference between the fit without the signal component and the default fit, which is 656, follows a  $\chi^2$  distribution with the number of degrees of freedom being the difference in the free parameters of the two fits, which is 4 [41]. The signal yield in the  $B^+ \rightarrow D^+ D^- K^+$  channel is obtained as  $N_{\text{norm}} = 3215 \pm 65$ , where the uncertainty is statistical, and the purity is around 91% using the same mass window definition. The  $B^+ \rightarrow D^+ D^- K^+$  signal yield is larger and the corresponding purity is lower compared with those in Refs. [11, 12], reflecting that looser selection criteria are imposed in this paper.

To demonstrate the potential contributions from intermediate resonances in the  $B^+ \rightarrow D_s^+ D_s^- K^+$  decay, the invariant-mass distributions of the  $D_s^+ D_s^-$ ,  $D_s^- K^+$  and  $D_s^+ K^+$

combinations, denoted respectively as  $m(D_s^+ D_s^-)$ ,  $m(D_s^- K^+)$  and  $m(D_s^+ K^+)$ , are shown in Fig. 3. The combinatorial background is subtracted using the *sPlot* method [42] with the  $B^+$  candidate mass exploited as the discriminating variable. A clear peaking structure is seen at the  $D_s^+ D_s^-$  mass threshold, corresponding to a charmonium(-like) candidate. An amplitude analysis is performed to study the resonant contributions in the  $B^+ \rightarrow D_s^+ D_s^- K^+$  decay, presented separately in Ref. [16]. The intermediate resonant contributions to the  $B^+ \rightarrow D^+ D^- K^+$  decay have been studied in the previous LHCb analyses described in Refs. [11, 12].

Pseudo-experiments are carried out to check potential biases on the extracted signal yields in the signal and normalisation channels. Numerous samples are randomly generated according to the determined PDFs where the number of signal (background) candidates in each sample is varied according to a Poissonian distribution with the mean set to the determined signal (background) yield, referred to as the default result. The signal yield in each generated sample is determined by a fit to the  $B^+$  candidate mass distribution and its variation from the default result is quantified as the pull value,  $(N_i - N_0)/\sigma_i$ , where  $N_i$  and  $\sigma_i$  are the signal yield and its statistical uncertainty in the  $i$ -th sample, respectively, and  $N_0$  is the default signal yield. The pull distribution is then fitted using a Gaussian function. The mean represents the bias on the signal yield relative to the size of its statistical uncertainty. The bias is  $\delta_{\text{sig}} = 0.09 \pm 0.01$  for the signal channel and is corrected for in the branching fraction calculation. Here, the uncertainty is due to limited number of the pseudo-experiments. No obvious bias is found on the signal yield for the normalisation channel.

The measured  $B^+ \rightarrow D_s^+ D_s^- K^+$  and  $B^+ \rightarrow D^+ D^- K^+$  signal yields contain residual NDC contributions, which need to be subtracted in the branching fraction calculation presented in Sec. 5. The expected NDC yields are estimated using the same method as that in Refs. [11, 12], based on the number of candidates in the  $D_{(s)}^\pm$  mass sidebands. The fractions of the NDC yields in the total  $B^+$  signal yields, are found to be  $f_{\text{NDC}}^{\text{sig}} = (5.2 \pm 2.7)\%$  and  $f_{\text{NDC}}^{\text{norm}} = (3.2 \pm 0.6)\%$  for the  $B^+ \rightarrow D_s^+ D_s^- K^+$  and  $B^+ \rightarrow D^+ D^- K^+$  channels, respectively. The uncertainties are due to the limited number of the candidates in the  $D_{(s)}^\pm$  mass sidebands. The larger NDC-background contamination in the  $B^+ \rightarrow D^+ D^- K^+$  channel compared with that in Refs. [11, 12] is due to relatively looser selection requirements in this paper.

## 5 Branching fraction calculation

The branching fraction of the  $B^+ \rightarrow D_s^+ D_s^- K^+$  decay is measured relative to that of the  $B^+ \rightarrow D^+ D^- K^+$  decay,

$$\mathcal{R} \equiv \frac{\mathcal{B}(B^+ \rightarrow D_s^+ D_s^- K^+)}{\mathcal{B}(B^+ \rightarrow D^+ D^- K^+)} = \frac{N_{\text{sig}}^{\text{corr}}}{N_{\text{norm}}^{\text{corr}}} \left[ \frac{\mathcal{B}(D^+ \rightarrow K^- \pi^+ \pi^+)}{\mathcal{B}(D_s^+ \rightarrow K^- K^+ \pi^+)} \right]^2, \quad (1)$$

where the branching fractions of the decays  $B^+ \rightarrow D^+ D^- K^+$ ,  $D^+ \rightarrow K^- \pi^+ \pi^+$  and  $D_s^+ \rightarrow K^- K^+ \pi^+$  are taken from Ref. [6, 14]. The efficiency-corrected signal yields of the

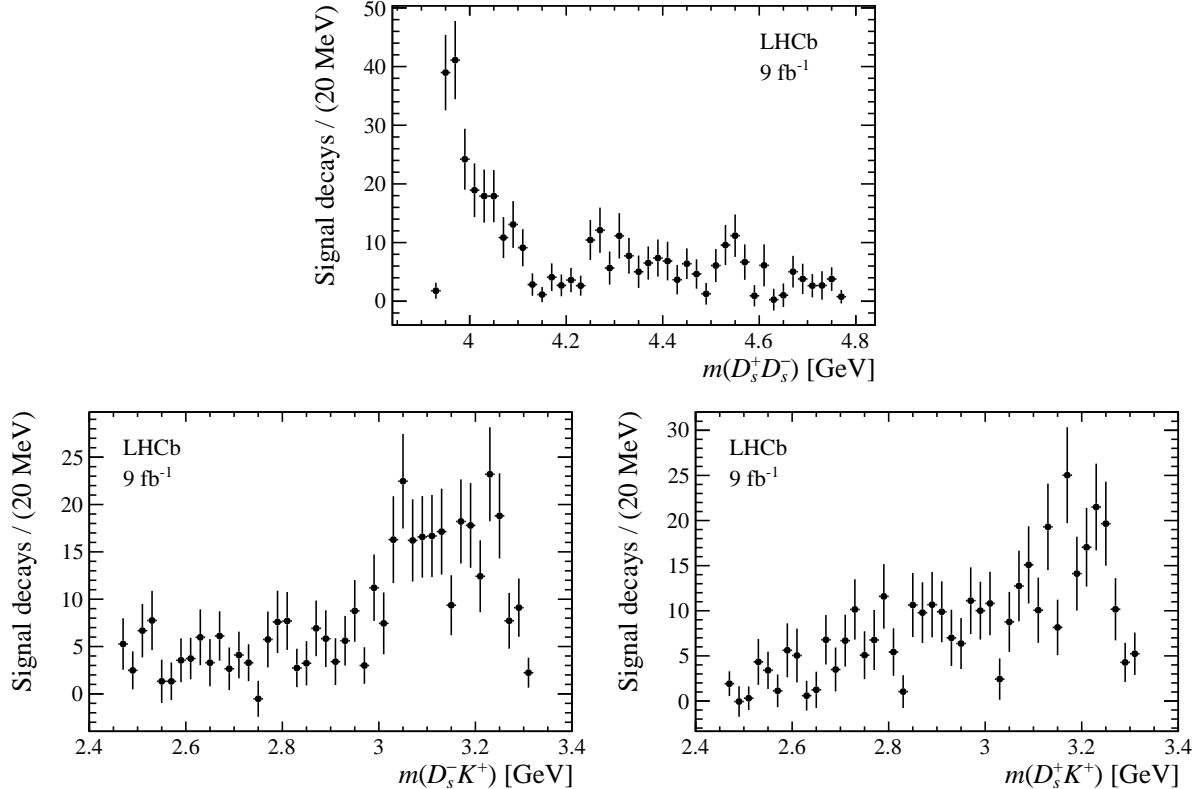


Figure 3: Distributions of background-subtracted invariant mass of the (top)  $D_s^+ D_s^-$ , (bottom left)  $D_s^- K^+$  and (bottom right)  $D_s^+ K^+$  systems of the  $B^+ \rightarrow D_s^+ D_s^- K^+$  decay.

$B^+ \rightarrow D_s^+ D_s^- K^+$  and  $B^+ \rightarrow D^+ D^- K^+$  channels,  $N_{\text{sig}}^{\text{corr}}$  and  $N_{\text{norm}}^{\text{corr}}$ , are determined as

$$N_{\text{sig}}^{\text{corr}} = \sum_i \frac{w_{\text{sig},i}}{\epsilon_{\text{sig},i}(m^2(D_s^+ D_s^-), m^2(D_s^- K^+))}, \quad (2)$$

$$N_{\text{norm}}^{\text{corr}} = \sum_i \frac{w_{\text{norm},i}}{\epsilon_{\text{norm},i}(m^2(D^+ D^-), m^2(D^- K^+))}, \quad (3)$$

where the index  $i$  runs over all the selected  $B^+$  candidates in the signal or normalisation channel. The weight  $w_{\text{sig},i}$  or  $w_{\text{norm},i}$  assigned to each candidate is obtained using the *sPlot* method [42]; summing over these weights effects a statistical subtraction of the combinatorial background contribution. The discriminating variable is the reconstructed  $D_s^+ D_s^- K^+$  or  $D^+ D^- K^+$  mass, as shown in Fig. 2. The efficiencies  $\epsilon_{\text{sig},i}$  and  $\epsilon_{\text{norm},i}$ , determined using simulated samples, take into account the effects of geometric acceptance, reconstruction and selection requirements. They are evaluated separately in the two data-taking periods, 2011–2012 (Run1) and 2015–2018 (Run2), and are shown in Fig. 4 as functions of the Dalitz-plot variables of the corresponding decays. The kernel density estimation (KDE) [43] technique is employed to obtain smooth efficiency distributions across the Dalitz plots. Finally, the efficiency-corrected yields are determined to be  $N_{\text{sig}}^{\text{corr}} = (9.5 \pm 0.6) \times 10^5$  and  $N_{\text{norm}}^{\text{corr}} = (5.33 \pm 0.11) \times 10^6$ , where the uncertainties are statistical only.

Before obtaining the branching-fraction ratio  $\mathcal{R}$ , it is necessary to subtract the NDC background contributions and to correct for the small fit bias on the extracted signal yield



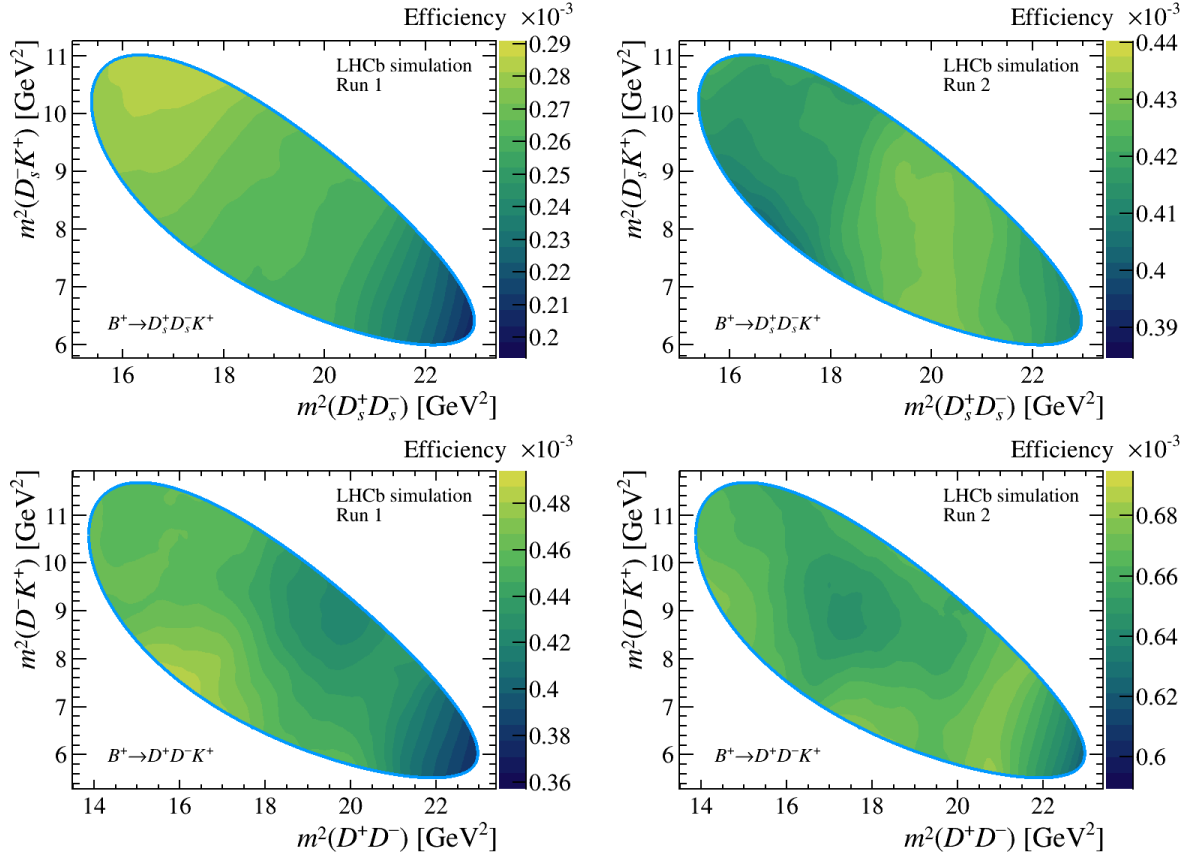


Figure 4: Efficiency as a function of the Dalitz-plot variables for the (top)  $B^+ \rightarrow D_s^+ D_s^- K^+$  and (bottom)  $B^+ \rightarrow D^+ D^- K^+$  decays, calculated separately for the (left) Run1 and (right) Run2 periods.

in the  $B^+ \rightarrow D_s^+ D_s^- K^+$  channel. These two effects are accounted for by introducing in Eq. 1 two correction factors:  $(1 - f_{\text{NDC}}^{\text{sig}})/(1 - f_{\text{NDC}}^{\text{norm}})$  for the NDC background subtraction, and  $1 - \sigma_{\text{sig}} \cdot \delta_{\text{sig}}/N_{\text{sig}}$  for the bias correction, where  $N_{\text{sig}} \pm \sigma_{\text{sig}} = 360 \pm 22$  and  $\delta_{\text{sig}} = 0.09$ . The branching-fraction ratio is determined to be

$$\mathcal{R} = 0.525 \pm 0.033, \quad (4)$$

where the uncertainty is due to statistical uncertainties on the efficiency-corrected yields of both the  $B^+ \rightarrow D_s^+ D_s^- K^+$  and  $B^+ \rightarrow D^+ D^- K^+$  channels.

## 6 Systematic uncertainties

The sources of the systematic uncertainty on the branching-fraction ratio are summarised in Table 1. They can be classified into two categories: the effects on the signal yields and the effects on the efficiencies. The total uncertainty is obtained by adding the contributions in quadrature.

The sources affecting the signal yields include the choice of the signal and background PDFs in the  $B^+$  mass fits, the uncertainties on the NDC background fractions in the signal and normalisation channels, the uncertainty on the bias of the  $B^+ \rightarrow D_s^+ D_s^- K^+$  signal

Table 1: Sources of systematic uncertainty on the branching-fraction ratio. The statistical uncertainty is also given.

Systematic source	Relative uncertainty (%)
Signal model	0.3
Background model	0.1
NDC background	2.9
Mass fit bias	0.1
Multiple-candidate removal	0.7
Hardware trigger correction	2.3
PID correction	2.8
Classifier modelling	1.6
Tracking	1.0
Truth matching	0.6
Limited size of simulated samples	0.5
KDE parameters	0.4
Total syst. (stat.)	5.1 (6.3)

yield and the multiple-candidate removal strategy. To evaluate the systematic uncertainty related to the choice of the signal PDF, an alternative model with a Hypatia function [44] is employed in the  $B^+$  mass fits to the signal and normalisation channels. The effect due to the choice of the background PDF is evaluated in a similar way, where a second-order polynomial function is used as an alternative. The NDC background fractions in the signal and normalisation channels have large uncertainties, which are due to the limited size of the data samples in the  $D^\pm$  and  $D_s^\pm$  mass sidebands. These uncertainties are propagated to the branching-fraction ratio. The uncertainty on the bias of the  $B^+ \rightarrow D_s^+ D_s^- K^+$  signal yield, resulting from the limited number of the pseudo-experiments that are employed to estimate the bias, is propagated in a similar way. Finally, the effect of the multiple-candidate removal strategy is evaluated by retaining an arbitrarily chosen candidate in an event.

The remaining systematic uncertainty sources in Table 1 influence the efficiencies in the signal and normalisation channels. The hardware trigger is generally not well modelled in the LHCb simulation but the effect is expected to largely cancel in the branching-fraction ratio thanks to the similarity in the topology between the signal and normalisation channels. The residual effect is evaluated by applying to the simulated events an event-by-event correction that is determined by calibration samples [45].

The PID responses is not well described in the simulation either and thus is corrected in the default result, with the correction determined from calibration samples using the PID transformation approach [34,35]. The performance of the correction is limited by the size of the calibration samples, the choice of the values of hyper parameters in the transformation approach and the choice of the correction approach itself. The corresponding effects are investigated by extracting the efficiency maps from simulated samples with the correction determined by using alternative calibration samples bootstrapped from the original ones, varying the values of the hyper parameters of the PID transformation approach, and choosing the PID resampling approach [34,35]. The resulting changes on the branching-fraction ratio are taken as the systematic uncertainties and are added in quadrature to

obtain the uncertainty due to the imperfect PID correction.

The potentially imperfect descriptions of the discriminating variables in the simulation can cause bias on the efficiencies of the BDTG classifiers. The effect is evaluated by varying the BDTG selection for the two channels and the resulting change of the branching-fraction ratio is taken as the systematic uncertainty.

The uncertainties on the tracking efficiencies for the same species of final-state particles in the signal and normalisation channels are expected to be the same and fully correlated, so their effects on the branching-fraction ratio largely cancel. The residual effect is from different final-state particles in the two channels, *i.e.*  $D_s^+ \rightarrow K^- K^+ \pi^+$  and  $D^+ \rightarrow K^- \pi^+ \pi^+$ . The systematic uncertainty on the branching-fraction ratio is evaluated as 1.0% [46, 47].

In the simulation, a truth-matching algorithm is used to identify signal decays. The efficiency of this algorithm is not 100%, leading to an underestimation of the efficiencies shown in Figure 4. However, the truth-matching efficiencies are expected to be very similar between the signal and normalisation channels, and thus the associated systematic uncertainties largely cancel. To evaluate the potential residual effect, the truth-matching efficiencies in the two channels are estimated using  $B^+$  mass fits to the simulated samples with and without truth matching. The efficiencies are introduced as correction factors to the branching-fraction ratio, and the resulting variation is taken as the systematic uncertainty.

The kernel width in the KDE method is chosen to be  $2 \text{ GeV}^2$  in the default result. To evaluate the systematic effect due to this choice, two alternative values,  $1 \text{ GeV}^2$  and  $3 \text{ GeV}^2$ , are taken in the efficiency parameterisations. The maximum change of the branching-fraction ratio is taken as the systematic uncertainty.

The last systematic uncertainty source affecting the efficiencies is the limited size of simulated samples. The uncertainty is propagated to the branching-fraction ratio using the bootstrap method [48]. Bootstrapped samples are produced by randomly selecting from the simulated candidates with replacement. Each such sample has the same size as the original simulated sample. These samples are employed to determine efficiencies and finally to obtain a set of branching-fraction ratios, whose standard deviation is taken as the systematic uncertainty.

## 7 Summary

In conclusion, the  $B^+ \rightarrow D_s^+ D_s^- K^+$  decay is observed for the first time using the proton–proton collision data collected by the LHCb detector at centre-of-mass energies of 7, 8 and 13 TeV, corresponding to an integrated luminosity of  $9 \text{ fb}^{-1}$ . The significance of the signal observed is larger than  $10 \sigma$ . The branching fraction of this decay is measured relative to that of the  $B^+ \rightarrow D^+ D^- K^+$  normalisation channel as

$$\mathcal{R} = \frac{\mathcal{B}(B^+ \rightarrow D_s^+ D_s^- K^+)}{\mathcal{B}(B^+ \rightarrow D^+ D^- K^+)} = 0.525 \pm 0.033 \pm 0.027 \pm 0.034. \quad (5)$$

With  $\mathcal{B}(B^+ \rightarrow D^+ D^- K^+) = (2.2 \pm 0.7) \times 10^{-4}$  as the input [6, 14], the  $B^+ \rightarrow D_s^+ D_s^- K^+$  branching fraction is then determined to be

$$\mathcal{B}(B^+ \rightarrow D_s^+ D_s^- K^+) = (1.15 \pm 0.07 \pm 0.06 \pm 0.38) \times 10^{-4}. \quad (6)$$

In each of these results, the first and second uncertainties are statistical and systematic, respectively, and the third is from the uncertainties on the known branching fractions of the  $D^+ \rightarrow K^- \pi^+ \pi^+$ ,  $D_s^+ \rightarrow K^- K^+ \pi^+$  and  $B^+ \rightarrow D^+ D^- K^+$  decays [6, 14].

The observation of the  $B^+ \rightarrow D_s^+ D_s^- K^+$  decay fills a major experimental gap in knowledge of the Cabibbo-favoured  $\bar{b} \rightarrow \bar{c} c \bar{s}$  transition with two open-charm hadrons in the final states [14]. The measurement of its branching fraction is of great importance for investigations of the intermediate resonant states. In particular, it is vital input to studies probing the nature of the near-threshold structure in the  $D_s^+ D_s^-$  system [16].

## References

- [1] A. Khodjamirian, T. Mannel, A. A. Pivovarov, and Y.-M. Wang, *Charm-loop effect in  $B \rightarrow K^{(*)} \ell^+ \ell^-$  and  $B \rightarrow K^* \gamma$* , JHEP **09** (2010) 089, [arXiv:1006.4945](#).
- [2] ALEPH collaboration, R. Barate *et al.*, *Observation of doubly charmed  $B$  decays at LEP*, Eur. Phys. J. **C4** (1998) 387.
- [3] BaBar collaboration, B. Aubert *et al.*, *Measurement of the branching fractions for the exclusive decays of  $B^0$  and  $B^+$  to  $\bar{D}^{(*)} D^{(*)} K$* , Phys. Rev. **D68** (2003) 092001, [arXiv:hep-ex/0305003](#).
- [4] BaBar collaboration, B. Aubert *et al.*, *Study of resonances in exclusive  $B$  decays to  $\bar{D}^{(*)} D^{(*)} K$* , Phys. Rev. **D77** (2008) 011102, [arXiv:0708.1565](#).
- [5] Belle collaboration, J. Brodzicka *et al.*, *Observation of a new  $D_{(s)J}$  meson in  $B^+ \rightarrow \bar{D}^0 D^0 K^+$  decays*, Phys. Rev. Lett. **100** (2008) 092001, [arXiv:0707.3491](#).
- [6] BaBar collaboration, P. del Amo Sanchez *et al.*, *Measurement of the  $B \rightarrow \bar{D}^{(*)} D^{(*)} K$  branching fractions*, Phys. Rev. **D83** (2011) 032004, [arXiv:1011.3929](#).
- [7] Belle collaboration, T. Aushev *et al.*, *Study of the decays  $B \rightarrow D_{s1}(2536)^+ \bar{D}^{(*)}$* , Phys. Rev. **D83** (2011) 051102, [arXiv:1102.0935](#).
- [8] BaBar collaboration, J. P. Lees *et al.*, *Dalitz plot analyses of  $B^0 \rightarrow D^- D^0 K^+$  and  $B^+ \rightarrow \bar{D}^0 D^0 K^+$  decays*, Phys. Rev. **D91** (2015) 052002, [arXiv:1412.6751](#).
- [9] LHCb collaboration, R. Aaij *et al.*, *First observation of the decay  $B^0 \rightarrow D^0 \bar{D}^0 K^+ \pi^-$* , Phys. Rev. **D102** (2020) 051102, [arXiv:2007.04280](#).
- [10] LHCb collaboration, R. Aaij *et al.*, *Measurement of branching fraction ratios for  $B^+ \rightarrow D^{*+} D^- K^+$ ,  $B^+ \rightarrow D^{*-} D^+ K^+$ , and  $B^0 \rightarrow D^{*-} D^0 K^+$  decays*, JHEP **12** (2020) 139, [arXiv:2005.10264](#).
- [11] LHCb collaboration, R. Aaij *et al.*, *Model-independent study of structure in  $B^+ \rightarrow D^+ D^- K^+$  decays*, Phys. Rev. Lett. **125** (2020) 242001, [arXiv:2009.00025](#).
- [12] LHCb collaboration, R. Aaij *et al.*, *Amplitude analysis of the  $B^+ \rightarrow D^+ D^- K^+$  decay*, Phys. Rev. **D102** (2020) 112003, [arXiv:2009.00026](#).

- [13] LHCb collaboration, R. Aaij *et al.*, *Observation of a new excited  $D_s^+$  state in  $B^0 \rightarrow D^- D^+ K^+ \pi^-$  decays*, Phys. Rev. Lett. **126** (2021) 122002, arXiv:2011.09112.
- [14] Particle Data Group, P. A. Zyla *et al.*, *Review of particle physics*, Prog. Theor. Exp. Phys. **2020** (2020) 083C01.
- [15] LHCb collaboration, R. Aaij *et al.*, *Observation of new resonances decaying to  $J/\psi K^+$  and  $J/\psi \phi$* , Phys. Rev. Lett. **127** (2021) 082001, arXiv:2103.01803.
- [16] LHCb collaboration, R. Aaij *et al.*, *Observation of a resonant structure near the  $D_s^+ D_s^-$  threshold in the  $B^+ \rightarrow D_s^+ D_s^- K^+$  decay*, arXiv:2210.15153, submitted to Phys. Rev. Lett.
- [17] LHCb collaboration, A. A. Alves Jr. *et al.*, *The LHCb detector at the LHC*, JINST **3** (2008) S08005.
- [18] LHCb collaboration, R. Aaij *et al.*, *LHCb detector performance*, Int. J. Mod. Phys. **A30** (2015) 1530022, arXiv:1412.6352.
- [19] R. Aaij *et al.*, *Performance of the LHCb Vertex Locator*, JINST **9** (2014) P09007, arXiv:1405.7808.
- [20] R. Arink *et al.*, *Performance of the LHCb Outer Tracker*, JINST **9** (2014) P01002, arXiv:1311.3893.
- [21] P. d'Argent *et al.*, *Improved performance of the LHCb Outer Tracker in LHC Run 2*, JINST **12** (2017) P11016, arXiv:1708.00819.
- [22] M. Adinolfi *et al.*, *Performance of the LHCb RICH detector at the LHC*, Eur. Phys. J. **C73** (2013) 2431, arXiv:1211.6759.
- [23] A. A. Alves Jr. *et al.*, *Performance of the LHCb muon system*, JINST **8** (2013) P02022, arXiv:1211.1346.
- [24] R. Aaij *et al.*, *The LHCb trigger and its performance in 2011*, JINST **8** (2013) P04022, arXiv:1211.3055.
- [25] V. V. Gligorov and M. Williams, *Efficient, reliable and fast high-level triggering using a bonsai boosted decision tree*, JINST **8** (2013) P02013, arXiv:1210.6861.
- [26] T. Likhomanenko *et al.*, *LHCb topological trigger reoptimization*, J. Phys. Conf. Ser. **664** (2015) 082025.
- [27] T. Sjöstrand, S. Mrenna, and P. Skands, *A brief introduction to PYTHIA 8.1*, Comput. Phys. Commun. **178** (2008) 852, arXiv:0710.3820; T. Sjöstrand, S. Mrenna, and P. Skands, *PYTHIA 6.4 physics and manual*, JHEP **05** (2006) 026, arXiv:hep-ph/0603175.
- [28] I. Belyaev *et al.*, *Handling of the generation of primary events in Gauss, the LHCb simulation framework*, J. Phys. Conf. Ser. **331** (2011) 032047.
- [29] D. J. Lange, *The EvtGen particle decay simulation package*, Nucl. Instrum. Meth. **A462** (2001) 152.

- [30] N. Davidson, T. Przedzinski, and Z. Was, *PHOTOS interface in C++: Technical and physics documentation*, Comp. Phys. Comm. **199** (2016) 86, [arXiv:1011.0937](#).
- [31] Geant4 collaboration, J. Allison *et al.*, *Geant4 developments and applications*, IEEE Trans. Nucl. Sci. **53** (2006) 270; Geant4 collaboration, S. Agostinelli *et al.*, *Geant4: A simulation toolkit*, Nucl. Instrum. Meth. **A506** (2003) 250.
- [32] M. Clemencic *et al.*, *The LHCb simulation application, Gauss: Design, evolution and experience*, J. Phys. Conf. Ser. **331** (2011) 032023.
- [33] D. Müller, M. Clemencic, G. Corti, and M. Gersabeck, *ReDecay: A novel approach to speed up the simulation at LHCb*, Eur. Phys. J. **C78** (2018) 1009, [arXiv:1810.10362](#).
- [34] L. Anderlini *et al.*, *The PIDCalib package*, LHCb-PUB-2016-021, 2016.
- [35] R. Aaij *et al.*, *Selection and processing of calibration samples to measure the particle identification performance of the LHCb experiment in Run 2*, Eur. Phys. J. Tech. Instr. **6** (2019) 1, [arXiv:1803.00824](#).
- [36] W. D. Hulsbergen, *Decay chain fitting with a Kalman filter*, Nucl. Instrum. Meth. **A552** (2005) 566, [arXiv:physics/0503191](#).
- [37] L. Breiman, J. H. Friedman, R. A. Olshen, and C. J. Stone, *Classification and regression trees*, Wadsworth international group, Belmont, California, USA, 1984.
- [38] Y. Freund and R. E. Schapire, *A decision-theoretic generalization of on-line learning and an application to boosting*, J. Comput. Syst. Sci. **55** (1997) 119.
- [39] H. Voss, A. Hoecker, J. Stelzer, and F. Tegenfeldt, *TMVA - Toolkit for Multivariate Data Analysis with ROOT*, PoS **ACAT** (2007) 040; A. Hoecker *et al.*, *TMVA 4 — Toolkit for Multivariate Data Analysis with ROOT. Users Guide.*, [arXiv:physics/0703039](#).
- [40] T. Skwarnicki, *A study of the radiative cascade transitions between the Upsilon-prime and Upsilon resonances*, PhD thesis, Institute of Nuclear Physics, Krakow, 1986, DESY-F31-86-02.
- [41] S. S. Wilks, *The large-sample distribution of the likelihood ratio for testing composite hypotheses*, Ann. Math. Stat. **9** (1938) 60.
- [42] M. Pivk and F. R. Le Diberder, *sPlot: A statistical tool to unfold data distributions*, Nucl. Instrum. Meth. **A555** (2005) 356, [arXiv:physics/0402083](#).
- [43] A. Poluektov, *Kernel density estimation of a multidimensional efficiency profile*, JINST **10** (2015) P02011, [arXiv:1411.5528](#).
- [44] D. Martínez Santos and F. Dupertuis, *Mass distributions marginalized over per-event errors*, Nucl. Instrum. Meth. **A764** (2014) 150, [arXiv:1312.5000](#).
- [45] A. Martin Sanchez, P. Robbe, and M.-H. Schune, *Performances of the LHCb L0 Calorimeter Trigger*, LHCb-PUB-2011-026, CERN-LHCb-PUB-2011-026, 2012.

- [46] LHCb collaboration, R. Aaij *et al.*, *Measurement of the branching fraction and CP asymmetry in  $B^+ \rightarrow J/\psi \rho^+$  decays*, Eur. Phys. J. **C79** (2019) 537, [arXiv:1812.07041](#).
- [47] LHCb collaboration, R. Aaij *et al.*, *Measurement of the branching fraction of the  $B^0 \rightarrow D_s^+ \pi^-$  decay*, Eur. Phys. J. **C81** (2021) 314, [arXiv:2010.11986](#).
- [48] B. Efron, *Bootstrap methods: Another look at the jackknife*, Ann. Statist. **7** (1979) 1.